

**Angles-Only Initial Relative-Orbit Determination via Successive Maneuvers**

by

Laura Marie Hebert

A thesis submitted to the Graduate Faculty of  
Auburn University  
in partial fulfillment of the  
requirements for the Degree of  
Master of Science

Auburn, Alabama  
May 7, 2016

Keywords: orbit determination, relative motion of satellites, angles-only navigation

Copyright 2016 by Laura Marie Hebert

Approved by

Andrew Sinclair, Chair, Associate Professor of Aerospace Engineering  
David Cicci, Professor of Aerospace Engineering  
John Cochran, Professor Emeritus of Aerospace Engineering  
T. Alan Lovell, Research Aerospace Engineer of the U.S. Air Force Research Laboratory

## Abstract

For relative-orbit determination using linear, Cartesian dynamics, angles-only measurements are not sufficient. A known, impulsive maneuver performed by either the observer or resident space object can provide observability. However, some maneuvers result in singular measurement equations and therefore do not provide full-state observability. These singular maneuvers can be avoided, but no further information can be provided about desirable maneuvers. The goal of this work is to provide an iterative method to improve observability and the accuracy of the solution. Successive maneuvers planned from covariance predictions using previous state estimates give increasingly good estimates.

## Acknowledgments

I'd like to thank my adviser, Dr. Sinclair, for sharing his knowledge and guidance in pursuing my masters degree. His patience and suggestions have proved invaluable to my research and this thesis. I'd also like to express my appreciation to Dr. Alan Lovell for introducing me to the topic of my research and for his support along the way, and to Dr. David Cicci and Dr. John Cochran for their guidance and for taking the time to serve on my committee. Finally, I am forever grateful to my parents, my sister Rebecca, and my fiancé Matt for all of their love and support along the way.

## Table of Contents

Abstract . . . . .	ii
Acknowledgments . . . . .	iii
List of Figures . . . . .	v
List of Tables . . . . .	vii
1 INTRODUCTION . . . . .	1
2 LINEAR DYNAMICS MODEL . . . . .	4
3 LINE OF SIGHT MEASUREMENTS . . . . .	9
3.1 Measurements from Reference Orbit . . . . .	10
3.2 Measurements from Homogeneous Observer . . . . .	11
4 INITIAL RELATIVE ORBIT DETERMINATION SOLUTION . . . . .	12
4.1 Maneuvering RSO . . . . .	13
4.2 Solution Accuracy . . . . .	14
5 MANEUVER DESIGN . . . . .	16
5.1 Singular Maneuvers . . . . .	16
5.1.1 Dependence of Solution Accuracy on Maneuver Design . . . . .	18
5.2 Multiple Maneuvers . . . . .	22
5.2.1 Example 1 . . . . .	23
5.2.2 Example 2 . . . . .	26
6 CONCLUSIONS . . . . .	30
Bibliography . . . . .	31

## List of Figures

2.1	Local Vertical Local Horizontal Coordinate System. . . . .	4
3.1	Family of Orbits with Identical Line of Sight Angle History. . . . .	10
5.1	Example observer maneuvers for two-dimensional IROD. . . . .	16
5.2	Observer maneuvers producing $0^\circ$ and $90^\circ$ changes in line-of-sight. . . . .	18
5.3	Contours of the determinant of $\mathbf{P}_x(t_4, \hat{\mathbf{x}}_0(t_4))$ , computed analytically. Maximum values have been artificially capped to show more detail in regions of low uncertainty. . . . .	19
5.4	Contours of the maximum eigenvalue of $\mathbf{P}_x(t_4, \hat{\mathbf{x}}_0(t_4))$ , computed analytically. Maximum values have been artificially capped to show more detail in regions of low uncertainty. . . . .	19
5.5	Contours of the determinant of $\mathbf{P}_x(t_4, \hat{\mathbf{x}}_0(t_4))$ . Maximum values have been artificially capped to show more detail in regions of low uncertainty. . . . .	20
5.6	Contours of the maximum eigenvalue of $\mathbf{P}_x(t_4, \hat{\mathbf{x}}_0(t_4))$ . Maximum values have been artificially capped to show more detail in regions of low error. . . . .	20
5.7	Contours of the maximum eigenvalue of $\mathbf{P}_x(t_4, \hat{\mathbf{x}}_0(t_4))$ , with higher simulated error. Maximum values have been artificially capped to show more detail in regions of low uncertainty. . . . .	21
5.8	Contours of the maximum eigenvalue of $\mathbf{P}_x(t_4, \hat{\mathbf{x}}_0(t_4))$ , with higher simulated error. Maximum values have been artificially capped to show more detail in regions of low uncertainty. . . . .	22

5.9 Contours of the determinant of  $\mathbf{P}_x(t_4, \hat{\mathbf{x}}(t_4), r_{obs}(t_4))$  after the first maneuver, with measurement errors. . . . . 24

5.10 Contours of the determinant of (a)  $\mathbf{P}_x(t_5, \hat{\mathbf{x}}(t_4), r_{obs}(t_5))$  used to design the second maneuver and (b)  $\mathbf{P}_x(t_5, \hat{\mathbf{x}}(t_5), r_{obs}(t_5))$  for after-the-fact reconstruction. . . . . 24

5.11 Contours of the determinant of (a)  $\mathbf{P}_x(t_6, \hat{\mathbf{x}}(t_5), r_{obs}(t_6))$  used to design the second maneuver and (b)  $\mathbf{P}_x(t_6, \hat{\mathbf{x}}(t_6), r_{obs}(t_6))$  for after-the-fact reconstruction. . . . . 25

5.12 Contours of the determinant of  $\mathbf{P}_x(t_4, \hat{\mathbf{x}}(t_4), r_{obs}(t_4))$  after the first maneuver, with measurement errors. . . . . 27

5.13 Contours of the determinant of (a)  $\mathbf{P}_x(t_5, \hat{\mathbf{x}}(t_4), r_{obs}(t_5))$  used to design the second maneuver and (b)  $\mathbf{P}_x(t_5, \hat{\mathbf{x}}(t_5), r_{obs}(t_5))$  for after-the-fact reconstruction. . . . . 28

5.14 Contours of the determinant of (a)  $\mathbf{P}_x(t_6, \hat{\mathbf{x}}(t_5), r_{obs}(t_6))$  used to design the second maneuver and (b)  $\mathbf{P}_x(t_6, \hat{\mathbf{x}}(t_6), r_{obs}(t_6))$  for after-the-fact reconstruction. . . . . 28

## List of Tables

5.1	Table of true initial states, $\mathbf{x}_0$ and estimates of initial states $\hat{\mathbf{x}}_0(t_4)$ , $\hat{\mathbf{x}}_0(t_5)$ , and $\hat{\mathbf{x}}_0(t_6)$ . . . . .	26
5.2	Table of true initial states, $\mathbf{x}_0$ and estimates of initial states $\hat{\mathbf{x}}_0(t_4)$ , $\hat{\mathbf{x}}_0(t_5)$ , and $\hat{\mathbf{x}}_0(t_6)$ . . . . .	29

## Chapter 1

### INTRODUCTION

Spacecraft formation flying can have benefits over a single spacecraft, as coordinating two or more satellites could allow each individual satellite to be built smaller and therefore less expensively. Flying in formation can also give a group of satellites more capability than a single satellite, by allowing an object to be viewed from multiple angles or at multiple times. A precise knowledge of the relative motion of satellites allows for formation flying, rendezvous, and docking. Angles-only navigation is necessary when taking range measurements is inadvisable or impossible, based on physical or mission constraints.

For certain relative navigation applications, it is desirable to perform initial relative-orbit determination using a minimal number of angles-only measurements. However, relative motion is unobservable when using angles-only measurements, and linear, Cartesian dynamics, and neither spacecraft is maneuvering.<sup>1,2</sup> Scalar multiples of the true initial state vector produce the same angle history.<sup>3</sup> The unknown satellite or resident space object could be on any member of a family of trajectories.

Previous work has been done in this area by Patel et al., who investigated methods to extract range-ambiguous solutions for the relative motion, and Newman et al., who investigated methods to generate complete solutions for the relative motion by using second-order nonlinear solutions for the relative motion, instead of linearized solutions.<sup>3,4</sup> This problem is similar to bearings-only tracking problems that have been extensively studied in the literature for other types of vehicles, with various dynamics. The use of maneuvers to gain observability of the range is particularly related to Ekelund ranging developed for submarines.<sup>5,6</sup> In a sense, this problem is also related to extensive work in dual control that investigates the coupling between estimation and control.<sup>7</sup> However, in the problem considered in this



work, control is used to aid estimation observability, but no other explicit control objective is considered.

While the mentioned limitations on observability are well understood, a simple presentation of how maneuvers allow for a unique solution has not previously been presented. This thesis demonstrates that a unique solution for the initial state vector can be found if one of the spacecraft performs a known maneuver in the midst of a minimal number of angles-only measurements.<sup>8</sup> This solution is found to have limitations in terms of singular maneuvers, and the maneuver choice affects the accuracy of the solutions. Certain maneuvers do not provide observability. These maneuvers result in a system of measurement equations that is singular. If a sufficient number of pre-maneuver measurements are available, then these singular maneuvers can be predicted before they are made and avoided.<sup>9</sup> In a related sense, in the presence of measurement errors, the design of the maneuver impacts the solution covariance. A priori it is not possible to predict the accuracy, but this thesis investigates an iterative approach of using successive maneuvers to achieve a desired level of solution covariance. After the first maneuver, and after the first solution estimate has been generated, this estimate can be used to predict the covariance associated with the estimate after a second maneuver.<sup>10</sup> And in this manner, the current estimate can be used in designing the subsequent maneuver.

This method is not intended to be an optimizer tool for a mission planner. It does not dictate a specific sequence of maneuvers, but provides information that may be used in choosing a maneuver. There is no explicit proof of robustness, but the law of least squares implies that more information always improves the estimate. The estimate of the initial states of a resident space object will converge given additional measurements.

The following chapters cover the method for estimating the initial state of an unknown satellite relative to the observer satellite. Chapter 2 covers the linear dynamics model, including some background on relative motion and the derivation of the nonlinear equations of motion. Chapter 3 describes collecting measurements, and the resulting measurement

equations. The initial relative orbit determination (IROD) solution, which can be found after performing the initial maneuver, is spelled out in Chapter 4, then Chapter 5 discusses maneuver design, and includes discussion of results and a couple of examples of solutions found using an iterative maneuver scheme.

## Chapter 2

### LINEAR DYNAMICS MODEL

Rather than referencing the motion of satellites to an inertial coordinate frame fixed to the center of the earth, as in the basic two-body problem of orbital mechanics, it can be useful to model the motion of one satellite, called the deputy, relative to a local-vertical local-horizontal (LVLH) coordinate frame fixed to another satellite, the chief. Within this LVLH frame, the position vector of the deputy relative to the chief has components  $x$ ,  $y$ , and  $z$ . Here,  $x$  lies along the chief's radial direction,  $z$  lies along the direction of the chief's orbital angular momentum, and  $y$  lies along the direction that completes the right-handed orthogonal coordinate system, as illustrated in Figure 2.1. The position vector from the center of the earth to the chief is called  $\mathbf{R}$ , and the inertial position vector of the deputy is called  $\mathbf{r}$ . The relative position vector from the chief to the deputy is denoted  $\boldsymbol{\rho}$ . The following equations describe the motion of the deputy and the chief in inertial space:

$$\mathbf{r} = \mathbf{R} + \boldsymbol{\rho} \quad (2.1)$$

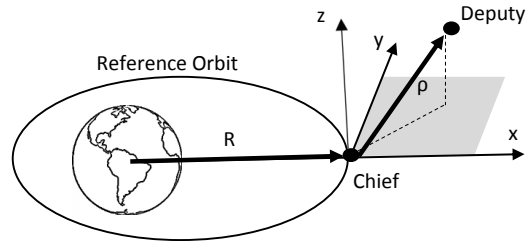


Figure 2.1: Local Vertical Local Horizontal Coordinate System.

$$\ddot{\mathbf{r}} = -\mu \frac{\mathbf{r}}{r^3} \quad (2.2)$$

$$\ddot{\mathbf{R}} = -\mu \frac{\mathbf{R}}{R^3} \quad (2.3)$$

Equation (2.2) is the inertial equation of motion for the deputy, and Eq. (2.3) is the inertial equation of motion for the chief. Here,  $\mu$  is the gravitational parameter. The equation of motion of the deputy with respect to the chief is found by substituting Eq. (2.1) into Eq. (2.2).

$$\ddot{\boldsymbol{\rho}} = -\ddot{\mathbf{R}} - \mu \frac{\mathbf{R} + \boldsymbol{\rho}}{r^3} \quad (2.4)$$

The magnitude of  $\boldsymbol{\rho}$  can be assumed to be very small compared to the magnitude of  $\mathbf{R}$ . Using this and Eq. (2.3) gives the linearized equation which governs the motion of the deputy relative to the chief, seen below:<sup>11</sup>

$$\ddot{\boldsymbol{\rho}} = \frac{-\mu}{R^3} \left[ \boldsymbol{\rho} - \frac{3}{R^2} (\mathbf{R} \cdot \boldsymbol{\rho}) \mathbf{R} \right] \quad (2.5)$$

Using  $\boldsymbol{\rho} = [\rho_x \ \rho_y \ \rho_z]$  to separate the above into scalar components results in the DeVries equations:<sup>14, 13, 12</sup>

$$\begin{aligned} \ddot{\rho}_x - \left( \frac{2\mu}{R^3} + \frac{h^2}{R^4} \right) \rho_x + \frac{2(\mathbf{V} \bullet \mathbf{R})h}{R^4} \rho_y - 2 \frac{h}{R^2} \dot{\rho}_y &= 0 \\ \ddot{\rho}_y + \left( \frac{\mu}{R^3} - \frac{h^2}{R^4} \right) \rho_y - \frac{2(\mathbf{V} \bullet \mathbf{R})h}{R^4} \rho_x + 2 \frac{h}{R^2} \dot{\rho}_x &= 0 \\ \ddot{\rho}_z + \frac{\mu}{R^3} \rho_z &= 0 \end{aligned} \quad (2.6)$$

In Eq. (2.6),  $h$  represents the angular momentum. Tschauner and Hempel applied a coordinate transformation and an independent-variable change to solve them.<sup>17</sup> If the eccentricity of the observer's orbit is zero, then the DeVries equations simplify to the Hill-Clohessy-Wiltshire (HCW) equations.<sup>15</sup> For a circular chief orbit,  $\mathbf{V} \bullet \mathbf{R} = 0$  and  $h = \sqrt{\mu R}$ . Substitute

both into Eq. (2.6), noting that angular velocity or mean motion is:

$$n = \sqrt{\frac{\mu}{R^3}} \quad (2.7)$$

This gives the HCW equations:

$$\begin{aligned} \ddot{\rho}_x - 3n^2\rho_x - 2n\dot{\rho}_y &= 0 \\ \ddot{\rho}_y + 2n\dot{\rho}_x &= 0 \\ \ddot{\rho}_z + n^2\rho_z &= 0 \end{aligned} \quad (2.8)$$

The first two equations are coupled, and describe the motion of the deputy in the  $xy$  plane. The third equation is independent of the others, so motion in the relative  $z$  direction does not depend on the other two directions.

To put Eq. (2.8) into matrix form, the relative state vector  $\mathbf{x}$  is defined as  $[\mathbf{r}^\top \mathbf{v}^\top]^\top = [x \ y \ z \ \dot{x} \ \dot{y} \ \dot{z}]^\top$ , then the solution to Eq. (2.8) in terms of the Hill-Clohessy-Wiltshire matrices is as follows:

$$\begin{bmatrix} \mathbf{r} \\ \mathbf{v} \end{bmatrix} = \begin{bmatrix} \Phi_{rr}(t, t_0) & \Phi_{rv}(t, t_0) \\ \Phi_{vr}(t, t_0) & \Phi_{vv}(t, t_0) \end{bmatrix} \begin{bmatrix} \mathbf{r}_0 \\ \mathbf{v}_0 \end{bmatrix} \quad (2.9)$$

$$[\Phi_{rr}(t, t_0)] = \begin{bmatrix} 4 - 3 \cos nt & 0 & 0 \\ 6 (\sin nt - nt) & 1 & 0 \\ 0 & 0 & \cos nt \end{bmatrix} \quad (2.10)$$

$$[\Phi_{rv}(t, t_0)] = \begin{bmatrix} \frac{1}{n} \sin nt & \frac{2}{n} (1 - \cos nt) & 0 \\ \frac{2}{n} (\cos nt - 1) & \frac{1}{n} (4 \sin nt - 3nt) & 0 \\ 0 & 0 & \frac{1}{n} \sin nt \end{bmatrix} \quad (2.11)$$

$$[\Phi_{vr}(t, t_0)] = \begin{bmatrix} 3n \sin nt & 0 & 0 \\ 6n (\cos nt - 1) & 0 & 0 \\ 0 & 0 & -n \sin nt \end{bmatrix} \quad (2.12)$$

$$[\Phi_{vv}(t, t_0)] = \begin{bmatrix} \cos nt & 2 \sin nt & 0 \\ -2 \sin nt & 4 \cos nt - 3 & 0 \\ 0 & 0 & \cos nt \end{bmatrix} \quad (2.13)$$

Equation (2.9) can also be partitioned as:

$$\begin{bmatrix} \mathbf{r} \\ \mathbf{v} \end{bmatrix} = \begin{bmatrix} \Phi_r(t, t_0) \\ \Phi_v(t, t_0) \end{bmatrix} \begin{bmatrix} \mathbf{r}_0 \\ \mathbf{v}_0 \end{bmatrix} \quad (2.14)$$

$$\mathbf{x}(t) = \Phi(t, t_0) \mathbf{x}_0 \quad (2.15)$$

The evolution of the state vector can be described by these linearized equations of motion.<sup>11, 12</sup>

The relative states can be linearly related to the unknown initial conditions using the HCW state-transition matrix.

Assuming a linear model is appropriate when the close separation distance between the two satellites is such that large errors do not develop due to the nonlinearity of the satellites true motion. The IROD solution will be based on the linearized model. Real motion,

however, obeys the full nonlinear equations, including perturbations. The small difference between these motions contributes process noise to the IROD solution.

In this work, the deputy is assumed to have unknown states and to be non-maneuvering, while the chief is assumed to have known states to be making known maneuvers. From here forward, the deputy will be referred to as a resident space object, or RSO, since this method could apply to any object in an orbit reasonably near the chief satellite. The chief satellite will be referred to as the observer satellite, and the orbit it is initially on is the reference orbit.

## Chapter 3

### LINE OF SIGHT MEASUREMENTS

Define the state vector for the RSO as  $\mathbf{x} = [\mathbf{r}_{RSO}^\top \mathbf{v}_{RSO}^\top]^\top$ . It is related to the unknown initial conditions by the state-transition matrix. The state vector for the observer is defined as  $\mathbf{y} = [\mathbf{r}_{obs}^\top \mathbf{v}_{obs}^\top]^\top$ , and is assumed to be known. The state and position of the RSO relative to the observer satellite is given by:

$$\mathbf{z} = \mathbf{x} - \mathbf{y} \quad (3.1)$$

$$\boldsymbol{\rho} = \mathbf{r}_{RSO} - \mathbf{r}_{obs} \quad (3.2)$$

Now take a line-of-sight measurement vector,  $\hat{\mathbf{u}} = [u_x \ u_y \ u_z]^\top$ , which is equal to a normalized version of the relative position plus noise,  $\delta\mathbf{u}$ . The measurement model is that the instantaneous relative position is parallel to  $\hat{\mathbf{u}}$ . This can be described by setting their cross product equal to zero.

$$\hat{\mathbf{u}} \times \boldsymbol{\rho} = \mathbf{0} \quad (3.3)$$

Alternatively, Eq. (3.3) can be rewritten as:

$$\hat{\mathbf{U}}\boldsymbol{\rho} \equiv \begin{bmatrix} 0 & -u_z & u_y \\ u_z & 0 & -u_x \\ -u_y & u_x & 0 \end{bmatrix} \begin{bmatrix} x \\ y \\ z \end{bmatrix} = \begin{bmatrix} 0 \\ 0 \\ 0 \end{bmatrix} \quad (3.4)$$

Note that only two of the three elements in the system of equations are independent.

Taking into account linear propagation of the initial conditions of the RSO and any motion by the observer, the relative position can be written as:

$$\boldsymbol{\rho} = \boldsymbol{\Phi}_r(t, t_0) \mathbf{x}_0 - \mathbf{r}_{obs}(t) \quad (3.5)$$



Inserting Eq. (3.5) into Eq. (3.4), the measurement equations can be rewritten as:

$$\hat{\mathbf{U}}\Phi_r(t, t_0)\mathbf{x}_0 = \hat{\mathbf{U}}\mathbf{r}_{obs}(t) \quad (3.6)$$

### 3.1 Measurements from Reference Orbit

For convenience, in this work, the reference orbit is defined as the observer’s orbit before performing any maneuvers. Therefore, the state of the observer,  $\mathbf{y}$ , is equal to  $\mathbf{0}$  prior to maneuvering. Collecting measurements from the reference orbit at multiple instances results in a system of equations of the form  $\mathbf{M}_1\mathbf{x}_0 = \mathbf{0}$ . For each new three-dimensional measurement taken,  $\mathbf{M}_1$  will gain three rows with six columns. Neglecting measurement and process noise,  $\mathbf{M}_1$  can be at most rank five, because the true state must satisfy the equations. The solution for  $\mathbf{x}_0$  must be parallel to the null vector. Therefore, the solution to these equations is magnitude ambiguous, as predicted by the previously observed limitations on angles-only observability. The RSO could be on any of a family of orbits, as demonstrated by Figure 3.1.

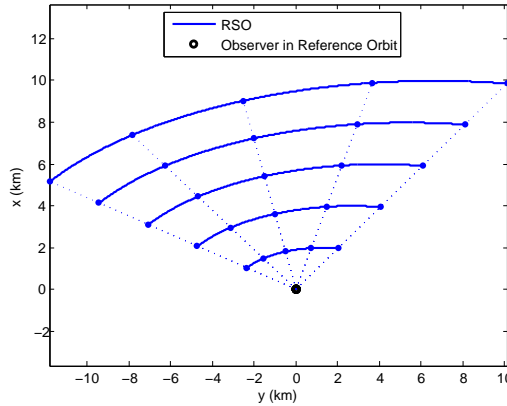


Figure 3.1: Family of Orbits with Identical Line of Sight Angle History.

### 3.2 Measurements from Homogeneous Observer

Consider an observer not located at the origin of the LVLH frame, but whose motion is described by the homogeneous linear dynamics:

$$\mathbf{r}_{obs}(t) = \Phi_r(t, t_0) \mathbf{y}_0 \quad (3.7)$$

We will refer to this as a homogeneous observer. Collecting measurements at multiple instants produces a system of equations in the form  $\mathbf{M}_2 \mathbf{x}_0 = \mathbf{b}$ , written in terms of the initial position of the RSO and the instantaneous position of the observer. Each measurement adds three rows of six columns for a three-dimensional formulation. It would appear that this system could give a unique solution for  $\mathbf{x}_0$ , but these equations could also be written in terms of  $\mathbf{z}_0$ :

$$\hat{U} \boldsymbol{\rho} = \hat{U} (\Phi_\rho \mathbf{x}_0 - \Phi_\rho \mathbf{y}_0) = \hat{U} \Phi_\rho \mathbf{z}_0 = \mathbf{0} \quad (3.8)$$

Therefore, multiple measurements from a homogeneous observer can be collected in the form of  $\mathbf{M}_1 \mathbf{z}_0 = \mathbf{0}$ , and there will not be a unique solution. In terms of the form  $\mathbf{M}_2 \mathbf{x}_0 = \mathbf{b}$ , this shows that  $\mathbf{M}_2$  is also at most rank five.

## Chapter 4

### INITIAL RELATIVE ORBIT DETERMINATION SOLUTION

A unique solution cannot be found assuming an observer on a single homogeneous trajectory, whether that trajectory is the origin or otherwise. An observer is required that inhabits multiple homogeneous trajectories, or in other words, a maneuvering observer. The matrix  $\mathbf{M}_2$  follows the same structure as  $\mathbf{M}_1$ , but the maneuver placing the observer on a different trajectory has changed the line-of-sight measurement. Concatenating measurement equations from before and after the maneuver gives the following system of linear equations.

$$\mathbf{M}\mathbf{x}_0 = \mathbf{b} \quad \mathbf{M} \equiv \begin{bmatrix} \mathbf{M}_1 \\ \mathbf{M}_2 \end{bmatrix} \quad \mathbf{b} = \begin{bmatrix} \mathbf{0} \\ \mathbf{b}_2 \end{bmatrix} \quad (4.1)$$

The matrix  $\mathbf{M}$  will generally have more rows than columns, so the system is overdetermined and therefore lacks a unique solution. An approximate least squares solution for  $\mathbf{x}_0$  is found by taking a pseudoinverse. The estimate for the initial states of the deputy is given by:

$$\hat{\mathbf{x}}_0 = (\mathbf{M}^\top \mathbf{M})^{-1} \mathbf{M}^\top \mathbf{b} \quad (4.2)$$

Each measurement equation only has three independent rows, but all three rows can be included in the pseudoinverse. A measurement at time  $t_k$  will be referred to as  $\mathbf{u}(t_k)$ . An estimate that takes into account the first  $k$  measurements is denoted as  $\hat{\mathbf{x}}_0(t_k)$ , or in full,  $\hat{\mathbf{x}}_0(\mathbf{u}(t_1), \mathbf{u}(t_2), \dots, \mathbf{u}(t_k))$ . The observer positions,  $\mathbf{r}_{obs}(t_1), \mathbf{r}_{obs}(t_2), \dots, \mathbf{r}_{obs}(t_k)$  are not included in the argument list for the sake of conciseness.

## 4.1 Maneuvering RSO

In the case that the observer remains at the origin and an RSO makes known maneuvers, this still produces changes in the line-of-sight just like an observer maneuver. Measurements before and after the maneuver can be combined and the initial state can still be calculated.

Since the equations are linear, the change in position of the deputy due only to the maneuver can be added to the motion due to the initial conditions.

$$\mathbf{r}_{RSO} = \Phi_r(t, t_0) \mathbf{x}_0 + \Phi_r(t, t_m) \begin{bmatrix} 0 \\ \Delta \mathbf{v} \end{bmatrix} \quad (4.3)$$

Use Eq. (3.2) to get an equation for  $\boldsymbol{\rho}$ .

$$\boldsymbol{\rho} = \Phi_r(t, t_0) \mathbf{x}_0 + \Phi_r(t, t_m) \begin{bmatrix} 0 \\ \Delta \mathbf{v} \end{bmatrix} - \mathbf{r}_{obs} \quad (4.4)$$

Since the observer does not maneuver,  $\mathbf{r}_{obs} = \mathbf{0}$ . Substitute Eq. (4.4) into Eq. (3.4) to get a measurement equation for a maneuvering RSO.

$$\hat{\mathbf{U}} \Phi_r(t, t_0) \mathbf{x}_0 = -\hat{\mathbf{U}} \Phi_r(t, t_m) \begin{bmatrix} 0 \\ \Delta \mathbf{v} \end{bmatrix} \quad (4.5)$$

Note that it is very similar to Eq. (3.6). This scenario could be incorporated easily in the same framework, but the engineering application is less clear. The active satellite is more often both the object that maneuvers and the object whose ephemeris is more accurately known. Thus the more common scenario is to consider the active satellite to be the observer, and is therefore not a focus of the subsequent discussion.

## 4.2 Solution Accuracy

Next, consider the presence of errors in the line-of-sight measurements. The line-of-sight vector  $\mathbf{u}$  has errors  $\delta\mathbf{u}$ . Since  $\mathbf{u}$  is a unit vector, there is no uncertainty along its direction, but there is uncertainty along the arc swept out by rotating the line-of-sight vector by an angle  $\delta\theta$ . For a unit vector, the arc length is equal to  $\delta\theta$  in radians. So the covariance for  $\mathbf{u}$  has principal components of zero along  $\mathbf{u}$  and  $\delta\theta^2$  along the directions perpendicular to  $\mathbf{u}$ . The measurement error covariance is then represented by the matrix  $\mathbf{R}$ , calculated by:<sup>16</sup>

$$\mathbf{R} = \mathbf{V}\mathbf{\Lambda}\mathbf{V}^\top \quad (4.6)$$

$$\mathbf{\Lambda} = \begin{bmatrix} 0 & 0 & 0 \\ 0 & \delta\theta^2 & 0 \\ 0 & 0 & \delta\theta^2 \end{bmatrix} \quad \mathbf{V} = \begin{bmatrix} \mathbf{u} & \mathbf{v} & \mathbf{w} \end{bmatrix} \quad (4.7)$$

$$\mathbf{u}^\top \mathbf{v} = \mathbf{u}^\top \mathbf{w} = \mathbf{v}^\top \mathbf{w} = 0 \quad (4.8)$$

Now the accuracy of the solution in the presence of these line-of-sight measurement errors can be considered. The covariance  $\mathbf{P}_x$  is a function of the measurements, the initial conditions of the RSO, and the observer positions. The covariance, taking into account measurements up through  $t_k$ , is defined as  $\mathbf{P}_x(\mathbf{u}(t_1), \mathbf{u}(t_2), \dots, \mathbf{u}(t_k), \mathbf{x}_0)$ , again leaving the dependence on  $\mathbf{r}_{obs}$  out of the argument list for the sake of conciseness. For an even more concise notation, covariance taking into account all measurements up through  $t_k$  will be defined as  $\mathbf{P}_x(t_k, \mathbf{x}_0)$ . The covariance will be developed by taking a first variation of the nonlinear measurement equations:

$$f(\mathbf{x}_0, \mathbf{u}_1, \dots, \mathbf{u}_n) = \mathbf{0} \quad (4.9)$$

$$\frac{\partial f}{\partial \mathbf{x}_0} \delta \mathbf{x}_0 + \sum_{i=1}^n \frac{\partial f}{\partial \hat{\mathbf{u}}_i} \delta \mathbf{u}_i = \mathbf{M} \delta \mathbf{x}_0 + \sum_{i=1}^n \mathbf{N}_i \delta \mathbf{u}_i = \mathbf{0} \quad (4.10)$$

$$\delta \mathbf{x}_0 = -(\mathbf{M}^\top \mathbf{M})^{-1} \mathbf{M}^\top \sum_{i=1}^n \mathbf{N}_i \delta \mathbf{u}_i \quad (4.11)$$

$$\begin{aligned} \mathbf{P}_x(t_k, \mathbf{x}_0) &= \mathbb{E}\{\delta \mathbf{x}_0 \delta \mathbf{x}_0^\top\} \\ &= \mathbb{E}\left\{(\mathbf{M}^\top \mathbf{M})^{-1} \mathbf{M}^\top \sum_{i=1}^n (\mathbf{N}_i \delta \mathbf{u}_i) \sum_{j=1}^n (\delta \mathbf{u}_j^\top \mathbf{N}_j^\top) \mathbf{M} (\mathbf{M}^\top \mathbf{M})^{-T}\right\} \\ &= (\mathbf{M}^\top \mathbf{M})^{-1} \mathbf{M}^\top \mathbb{E}\left\{\sum_{i=1}^n (\mathbf{N}_i \delta \mathbf{u}_i \delta \mathbf{u}_i^\top \mathbf{N}_i^\top)\right\} \mathbf{M} (\mathbf{M}^\top \mathbf{M})^{-T} \quad (4.12) \\ &= (\mathbf{M}^\top \mathbf{M})^{-1} \mathbf{M}^\top \sum_{i=1}^n (\mathbf{N}_i \mathbb{E}\{\delta \mathbf{u}_i \delta \mathbf{u}_i^\top\} \mathbf{N}_i^\top) \mathbf{M} (\mathbf{M}^\top \mathbf{M})^{-T} \\ &= (\mathbf{M}^\top \mathbf{M})^{-1} \mathbf{M}^\top \sum_{i=1}^n (\mathbf{N}_i \mathbf{R}_i \mathbf{N}_i^\top) \mathbf{M} (\mathbf{M}^\top \mathbf{M})^{-T} \end{aligned}$$

In the above, it was further assumed that the error in each line-of-sight measurement is independent from the error in any other line-of-sight measurement. Note that  $\mathbf{M}$  is an explicit function of all of the line-of-sight measurements (and therefore an implicit function of the RSO and observer motions), and  $\mathbf{N}$  is an explicit function of the RSO and observer motions. Further note, Eq. (4.11) indicates that unbiased measurements will produce an unbiased estimate. A higher-order expansion could be considered to more accurately compute the expected bias, but this is not pursued in this thesis.

## Chapter 5

### MANEUVER DESIGN

The analysis in the previous section described how the solution covariance is a function of the observer motion, which indicates that maneuver design will influence the solution accuracy. However, the covariance is also a function of the unknown motion of the RSO. Therefore, maneuver design cannot be performed by directly selecting a desired covariance value.

#### 5.1 Singular Maneuvers

Certain maneuvers should be avoided. Singular maneuvers result when the line-of-sight from the observer to the RSO after a maneuver is no different from the expected line-of-sight had no maneuver been performed. The change in line-of-sight generated by the maneuver is what provides observability. This is illustrated for a two-dimensional case in Figure 5.1.

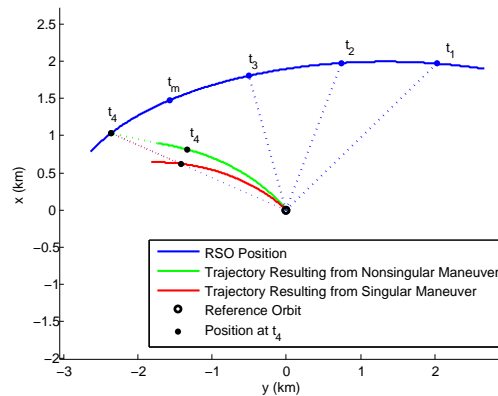


Figure 5.1: Example observer maneuvers for two-dimensional IROD.

To solve for a singular maneuver, consider a three-dimensional case with measurements collected at times  $t_1$  and  $t_2$  before  $t_m$ , and time  $t_3$  after  $t_m$ .

$$\mathbf{r}_{RSO}(t_3) = \Phi_r(t_3, t_0)\mathbf{x}_0 \quad (5.1)$$

$$\mathbf{r}_{obs} = \Phi_r(t_3, t_m) \begin{bmatrix} \mathbf{0} \\ \Delta\mathbf{v} \end{bmatrix} \quad (5.2)$$

The condition for singularity of  $\mathbf{M}$  is that:

$$\mathbf{r}_{obs}(t_3) = \alpha\mathbf{r}_{RSO}(t_3) \quad (5.3)$$

Therefore, the relative position vector at  $t_3$  is proportional to the relative position vector that would have resulted if no maneuver was performed, because the maneuver has not caused any change in the line-of-sight. Inserting Eq. (5.1) and (5.2) into Eq. (5.3), the manifold of singular maneuvers is then given by:

$$\Delta\mathbf{v}_s = \alpha\Phi_{rv}^{-1}(t_3, t_m)\mathbf{r}_{RSO}(t_3) \quad (5.4)$$

Computing the singular direction only requires the direction of the RSO position. With sufficient pre-maneuver measurements, this direction can be calculated.

Intuitively, the desirable location to obtain the most accurate estimate of the initial condition vector is orthogonal to the singular line-of-sight at the location of the RSO, as shown in Figure 5.2. This is validated by the covariance analysis, seen in Eq. (4.12). Unfortunately, both the range of the RSO and the covariance of the solution cannot be predicted until after a maneuver is made. Figures 5.1 and 5.2 are both generated with full knowledge of the true states.



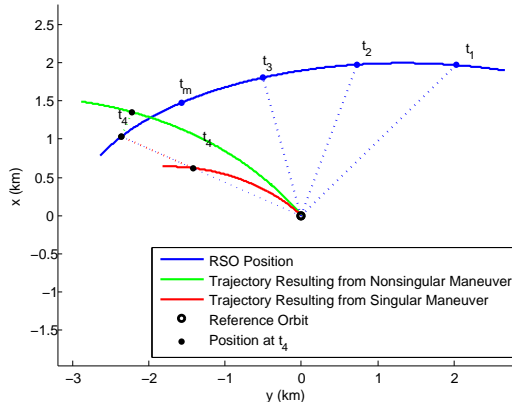


Figure 5.2: Observer maneuvers producing  $0^\circ$  and  $90^\circ$  changes in line-of-sight.

### 5.1.1 Dependence of Solution Accuracy on Maneuver Design

The covariance contours plotted in Figure 5.3 also support placing the observer orthogonal to the singular line-of-sight at the location of the RSO.  $\mathbf{P}_x$  is a function of the observer motion, and so this is a plot evaluating  $\mathbf{P}_x$  at a range of possible observer positions. Using both numerical investigation and intuitive insight, the behavior of  $\mathbf{P}_x(t_4, \hat{\mathbf{x}}_0(t_4))$  can be easier to visualize for two-dimensional motion with  $z = \dot{z} = 0$ . In this case, each observation consists of a line of sight vector  $\hat{u}$ , and four observations are required to solve for the four-dimensional initial state vector. Here, a sequence of three observations at  $t_1$ ,  $t_2$ , and  $t_3$ , then a maneuver at  $t_m$ , and finally an observation at  $t_4$  will be illustrated.

For a numerical simulation of  $\mathbf{P}_x$  for a range of  $r_{obs}(t_4)$  values, a circular reference orbit with semimajor axis of 6778 km is considered, with true initial conditions of  $x_0 = 1.9694402770846864$  km,  $y_0 = 2.0285452000386378$  km,  $\dot{x}_0 = 0.0003258380106737$  km/s, and  $\dot{y}_0 = -0.0042735407112798$  km/s. The measurement and maneuver times occur every five minutes; at  $t_1 = 0$  s,  $t_2 = 300$  s,  $t_3 = 600$  s,  $t_{m1} = 900$  s, and  $t_4 = 1200$  s. For a range of  $r_{obs}(t_4)$  values, the true values of line of sight measurements are simulated, and  $\mathbf{P}_x(t_4, \hat{\mathbf{x}}_0(t_4))$  is evaluated, assuming zero-mean, Gaussian measurement errors with standard deviation of

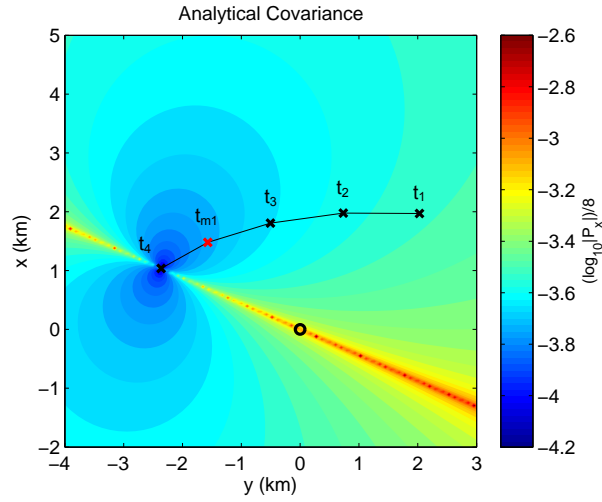


Figure 5.3: Contours of the determinant of  $\mathbf{P}_x(t_4, \hat{\mathbf{x}}_0(t_4))$ , computed analytically. Maximum values have been artificially capped to show more detail in regions of low uncertainty.

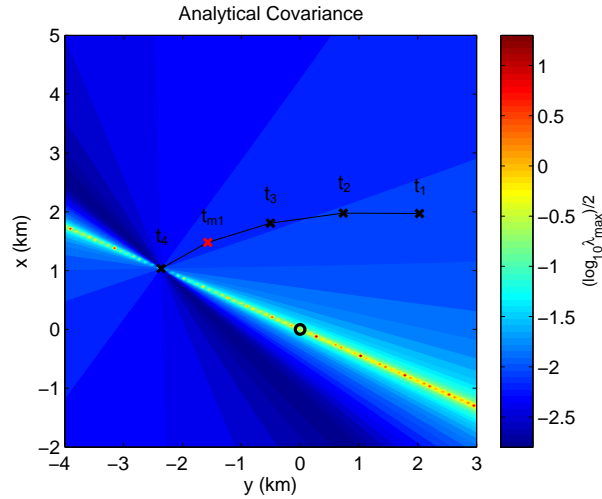


Figure 5.4: Contours of the maximum eigenvalue of  $\mathbf{P}_x(t_4, \hat{\mathbf{x}}_0(t_4))$ , computed analytically. Maximum values have been artificially capped to show more detail in regions of low uncertainty.

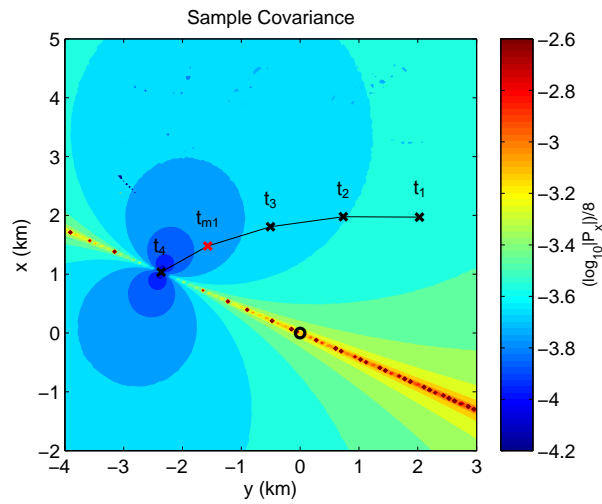


Figure 5.5: Contours of the determinant of  $\mathbf{P}_x(t_4, \hat{\mathbf{x}}_0(t_4))$ . Maximum values have been artificially capped to show more detail in regions of low uncertainty.

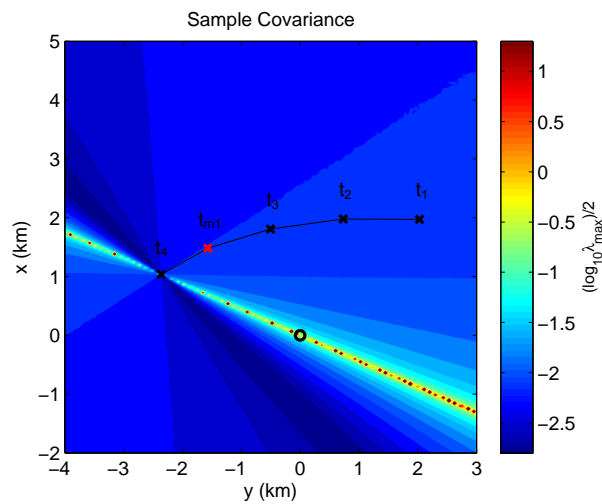


Figure 5.6: Contours of the maximum eigenvalue of  $\mathbf{P}_x(t_4, \hat{\mathbf{x}}_0(t_4))$ . Maximum values have been artificially capped to show more detail in regions of low error.

$5 \times 10^{-5}$  rad. Since this is in two dimensions, there are four states and each measurement has one independent component, three measurements are needed before the first maneuver in order to compute the singular direction. Contours of the determinant of  $\mathbf{P}_x(t_4, \hat{\mathbf{x}}_0(t_4))$  are shown in Figure 5.3, and Figure 5.4 shows contours of the maximum eigenvalue of  $\mathbf{P}_x(t_4, \hat{\mathbf{x}}_0(t_4))$ . Because these values are plotted over physical space, the true motion of the deputy is also superimposed, with the deputy's position at  $t_1$ ,  $t_2$ ,  $t_3$ , and  $t_4$  shown with black  $\times$ 's and the deputy's position at  $t_m$  shown with a red  $\times$ .

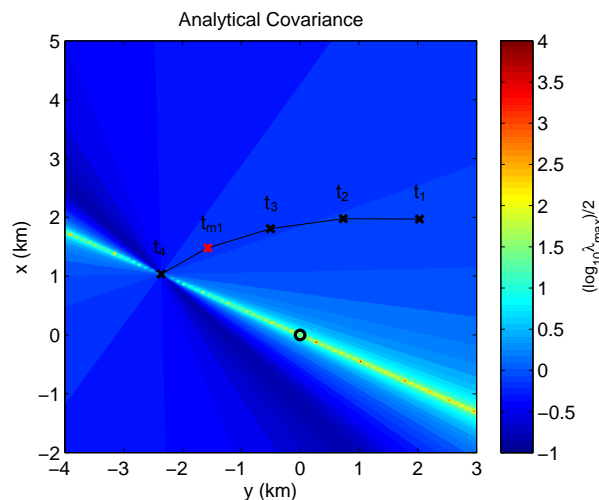


Figure 5.7: Contours of the maximum eigenvalue of  $\mathbf{P}_x(t_4, \hat{\mathbf{x}}_0(t_4))$ , with higher simulated error. Maximum values have been artificially capped to show more detail in regions of low uncertainty..

To verify the analytical values of the covariance, Monte Carlo simulations are also conducted. At each grid point for  $\mathbf{r}_{obs}(t_4)$ , 100,000 trials are conducted with different values of measurement error drawn from the described probability distribution. From the resulting population of solutions for  $\hat{\mathbf{x}}_0(t_4)$ , the sample covariance is calculated, and from comparison with the true value, the mean error is determined. Contours of these values are shown in Figures 5.5 and 5.6. These figures show good agreement with the analytical values.

The contours of the maximum eigenvalues of  $\mathbf{P}_x(t_4)$  and  $\bar{\delta \hat{\mathbf{x}}_0}$  both show asymmetric behavior with certain directions being preferred over others. The fact that these two plots show similar behavior is as expected. The largest eigenvalue is typically associated with

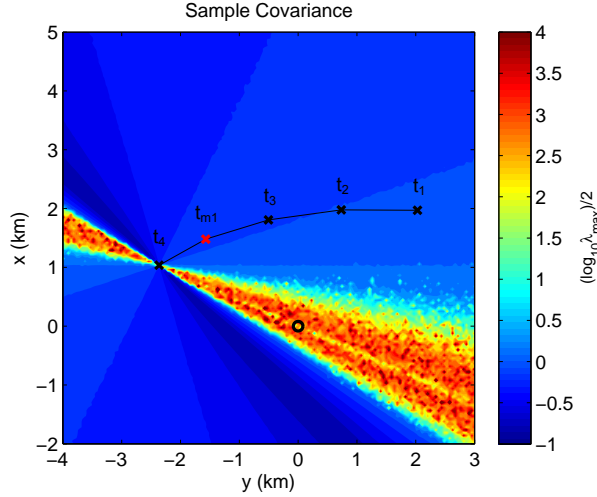


Figure 5.8: Contours of the maximum eigenvalue of  $\mathbf{P}_x(t_4, \hat{\mathbf{x}}_0(t_4))$ , with higher simulated error. Maximum values have been artificially capped to show more detail in regions of low uncertainty.

large uncertainty in the radial direction, and these radial uncertainties lead to triangulation bias. Chief positions that reduce the radial uncertainty will also reduce the bias.

Covariance plots were also generated with higher simulated measurement error. Contours of the maximum eigenvalue of  $\mathbf{P}_x$  are shown in Figure 5.7. The sample covariance was also calculated, and contours of the maximum eigenvalue of  $\mathbf{P}_x$  are shown in Figure 5.8, both calculated with a standard deviation of  $5 \times 10^{-3}$  rad. The analytical covariance in Eq. (4.12) was based on a linearized analysis, and it starts to break down for large measurement errors, as can be seen in the noisier plots generated using higher error.

## 5.2 Multiple Maneuvers

Covariance is a function of the RSO motion, and the plots in the previous section were generated using full knowledge of that motion. Since RSO motion is in reality unknown, it is impossible to choose a maneuver in order to provide optimal observability. So a small maneuver in a direction perpendicular to the singular direction is assumed. A known maneuver will enable an estimate of the initial conditions of the RSO,  $\hat{\mathbf{x}}_0$ , from which the covariance and bias may be evaluated. Using the  $\hat{\mathbf{x}}_0$  calculated from the first maneuver, along with the

state transition matrix,  $\Phi$ , the expected line-of-sight at a subsequent, desired measurement time may be found. These can then be used to calculate the expected covariance for a range of candidate maneuvers. Notation used to describe a covariance at a future point in time using currently available estimates will be  $\mathbf{P}_x(t_k, \hat{\mathbf{x}}_0(t_j, \mathbf{r}_{obs}(t_j)), \mathbf{r}_{obs}(t_k))$ , where  $t_j$  is a time occurring before time  $t_k$ . A second maneuver may then be chosen to improve the accuracy of the estimate,  $\hat{\mathbf{x}}_0$ . This process can be repeated for third and subsequent maneuvers, until a desired accuracy has been attained. For each post-maneuver measurement, a row is added to the  $\mathbf{M}_2$  matrix.

For easier visualization, the successive maneuver process is carried out in two dimensions for coplanar observer and RSO orbits. In two dimensional space, each line-of-sight measurement only produces one independent component. A circular reference orbit with semimajor axis of 6778 km is considered, and the true initial condition is chosen as  $x_0 = 1.9694402770846864$  km,  $y_0 = 2.0285452000386378$  km,  $\dot{x}_0 = 0.0003258380106737$  km/s, and  $\dot{y}_0 = -0.0042735407112798$  km/s. The measurement and maneuver times occur every five min;  $t_1 = 0$  s,  $t_2 = 300$  s,  $t_3 = 600$  s,  $t_{m1} = 900$  s,  $t_4 = 1200$  s,  $t_{m2} = 1500$  s,  $t_5 = 1800$  s,  $t_{m3} = 2100$  s, and  $t_6 = 2400$  s. For a range of  $r_{obs}(t_4)$  values, the true values of  $\mathbf{u}(t_4)$  are simulated, and  $\mathbf{P}_x$  is evaluated, assuming zero-mean, Gaussian measurement errors with standard deviation of  $5 \times 10^{-6}$  rad. Since this is in two dimensions there are four states and each measurement has one independent component, so three measurements are needed before the first maneuver in order to compute the singular direction.

The position of the observer after the first maneuver is chosen such that it is orthogonal to the singular line-of-sight at the fourth measurement time, and such that the maneuver is small, with a magnitude of 1 cm/s.

### 5.2.1 Example 1

In Figure 5.9, the estimated trajectory of the RSO is plotted, up to the time of the fourth measurement. The final position of the observer after the first maneuver is represented by a

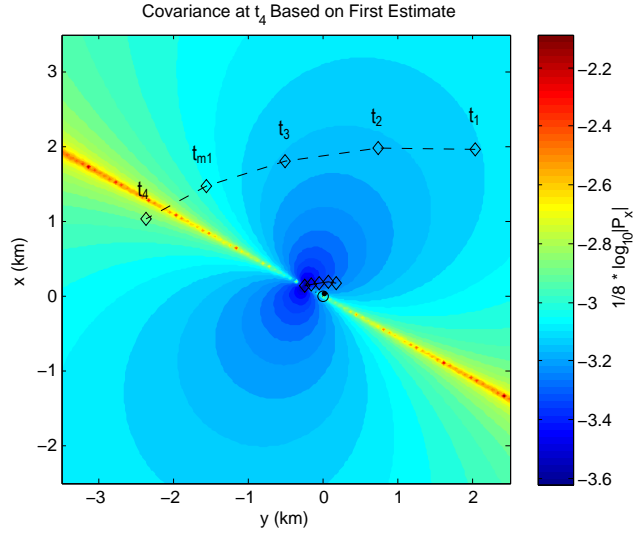


Figure 5.9: Contours of the determinant of  $\mathbf{P}_x(t_4, \hat{\mathbf{x}}(t_4), r_{obs}(t_4))$  after the first maneuver, with measurement errors.

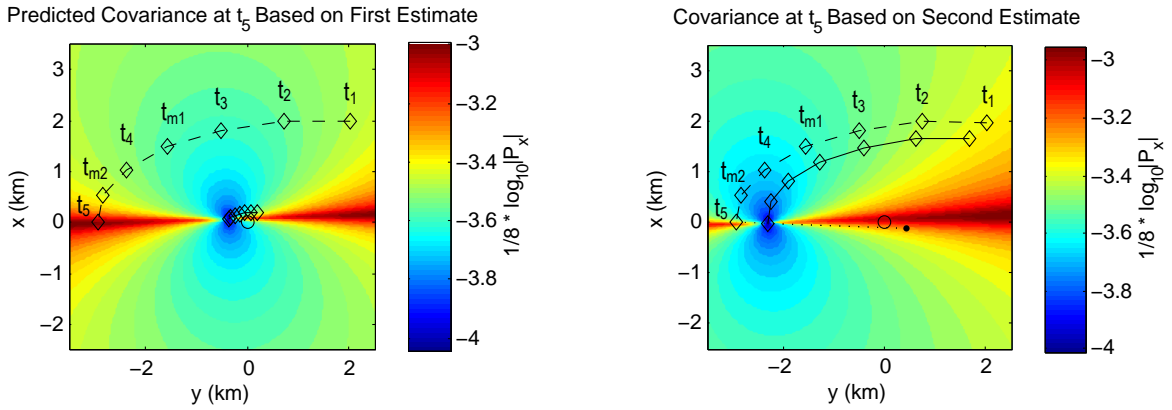


Figure 5.10: Contours of the determinant of (a)  $\mathbf{P}_x(t_5, \hat{\mathbf{x}}(t_4), r_{obs}(t_5))$  used to design the second maneuver and (b)  $\mathbf{P}_x(t_5, \hat{\mathbf{x}}(t_5), r_{obs}(t_5))$  for after-the-fact reconstruction.

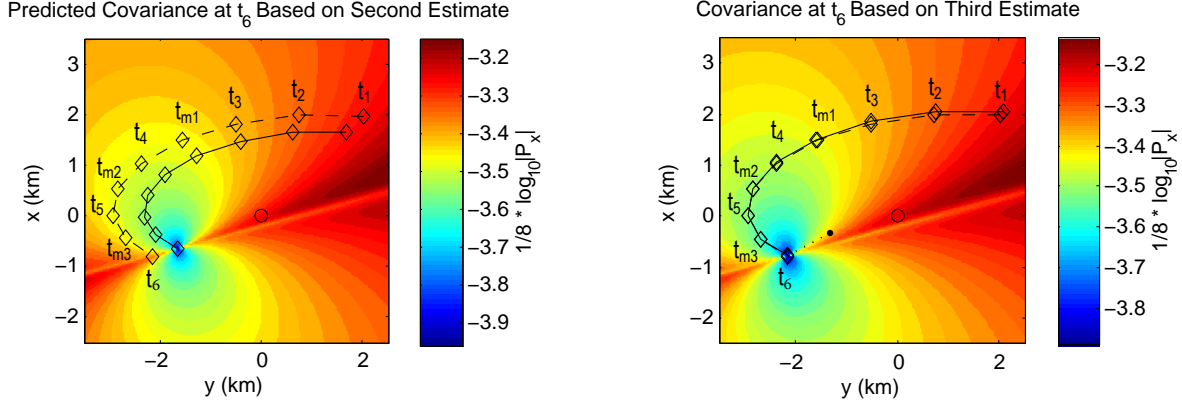


Figure 5.11: Contours of the determinant of (a)  $\mathbf{P}_x(t_6, \hat{x}(t_5), r_{obs}(t_6))$  used to design the second maneuver and (b)  $\mathbf{P}_x(t_6, \hat{x}(t_6), r_{obs}(t_6))$  for after-the-fact reconstruction.

black point. The covariance after measurement 4 is shown below.

$$|\mathbf{P}_x(t_4, \hat{x}(t_4))| = 1.4548 \times 10^{-25} \quad (5.5)$$

Figure 5.10(a) shows predictions of the covariance after measurement 5 based on possible positions for a second post-maneuver measurement. These covariance predictions are calculated using the estimate produced from measurements 1-4. They allow for planning of the second maneuver. The black dot in Figure 5.10 represents one choice for the second post-maneuver position. After collection of measurement 5, the covariance is found to be:

$$|\mathbf{P}_x(t_5, \hat{x}(t_5))| = 1.7872 \times 10^{-26} \quad (5.6)$$

The reconstruction of the covariance at  $t_5$  using the updated estimate is shown in Figure 5.10(b). Figure 5.11(a) shows predictions of the covariance after measurement 6. The



	$\mathbf{x}_0$	$\hat{\mathbf{x}}_0(t_4)$	$\hat{\mathbf{x}}_0(t_5)$	$\hat{\mathbf{x}}_0(t_6)$
$\mathbf{r}$	1.9694	1.9236	1.9700	1.9691
	2.0285	1.9813	2.0290	2.0282
$\mathbf{v}$	0.0003	0.0003	0.0003	0.0003
	-0.0043	-0.0042	-0.0043	-0.0043

Table 5.1: Table of true initial states,  $\mathbf{x}_0$  and estimates of initial states  $\hat{\mathbf{x}}_0(t_4)$ ,  $\hat{\mathbf{x}}_0(t_5)$ , and  $\hat{\mathbf{x}}_0(t_6)$ .

covariance predictions are calculated using the estimate produced from the previous five measurements. The third maneuver can be planned based on these. The black dot in Figure 5.11(b) represents one choice for the second post-maneuver position. The covariance after measurement 6 is:

$$|\mathbf{P}_x(t_6, \hat{\mathbf{x}}(t_6))| = 9.5145 \times 10^{-28} \quad (5.7)$$

The reconstruction of the covariance at  $t_6$  using the updated estimate is shown in Figure 5.11(b). Table 5.1 includes estimates of  $\mathbf{x}_0$  calculated after  $t_{m1}$ ,  $t_{m2}$ , and  $t_{m3}$ . Clearly, estimates improve after each new maneuver.

### 5.2.2 Example 2

Now consider an example with the same true initial condition and distribution of measurement errors, but a different random draw from that error distribution. In this case, the first maneuver results in an estimate of the initial state vector of the RSO that is not only the magnitude, but 180° in the wrong direction, as seen in Figure 5.12. The covariance after measurement 4 is:

$$|\mathbf{P}_x(t_4, \hat{\mathbf{x}}(t_4))| = 1.6631 \times 10^{-23} \quad (5.8)$$

The direction ambiguity is removed by a second measurement, planned using Figure 5.13(a). The second estimate, calculated from the all of the data collected up through measurement 5, is seen to be in the correct direction, if still inaccurate in range, in Figure 5.13(b). The

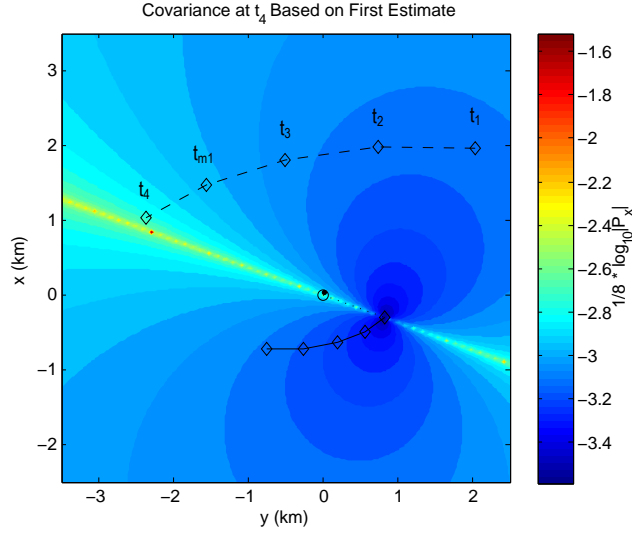


Figure 5.12: Contours of the determinant of  $\mathbf{P}_x(t_4, \hat{\mathbf{x}}(t_4), r_{obs}(t_4))$  after the first maneuver, with measurement errors.

covariance after measurement 5 is found to be:

$$|\mathbf{P}_x(t_5, \hat{\mathbf{x}}(t_5))| = 2.2059 \times 10^{-26} \quad (5.9)$$

The third maneuver is designed using Figure 5.14(a) and executed such that the position of the observer satellite at the time of the measurement 6 is in the location marked by the black dot in Figure 5.14(b). The final covariance is:

$$|\mathbf{P}_x(t_6, \hat{\mathbf{x}}(t_6))| = 3.5118 \times 10^{-28} \quad (5.10)$$

It can be seen that the estimate of the RSO initial states that includes this final maneuver is much closer to the correct value than the first estimate.

Table 5.2 includes estimates of  $\mathbf{x}_0$  calculated after  $t_{m1}$ ,  $t_{m2}$ , and  $t_{m3}$ . Again, estimates improve after each new maneuver.

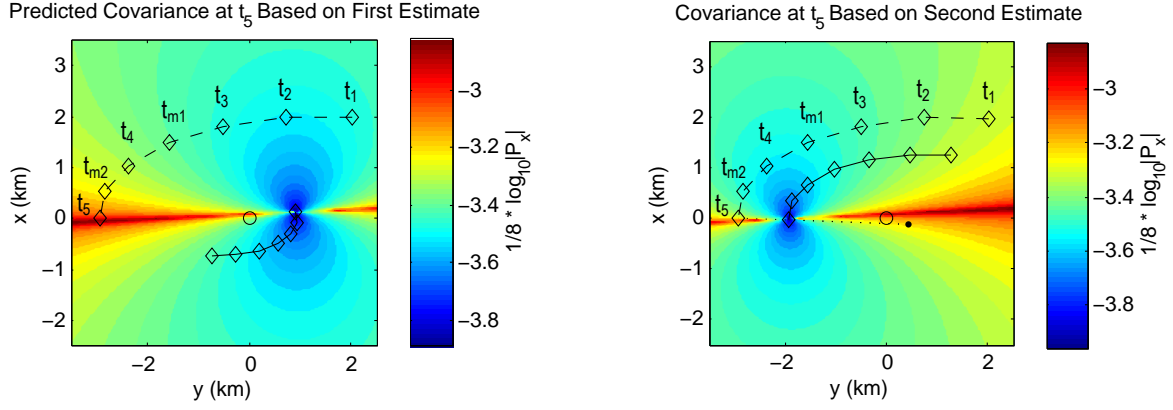


Figure 5.13: Contours of the determinant of (a)  $\mathbf{P}_x(t_5, \hat{x}(t_4), r_{obs}(t_5))$  used to design the second maneuver and (b)  $\mathbf{P}_x(t_5, \hat{x}(t_5), r_{obs}(t_5))$  for after-the-fact reconstruction.

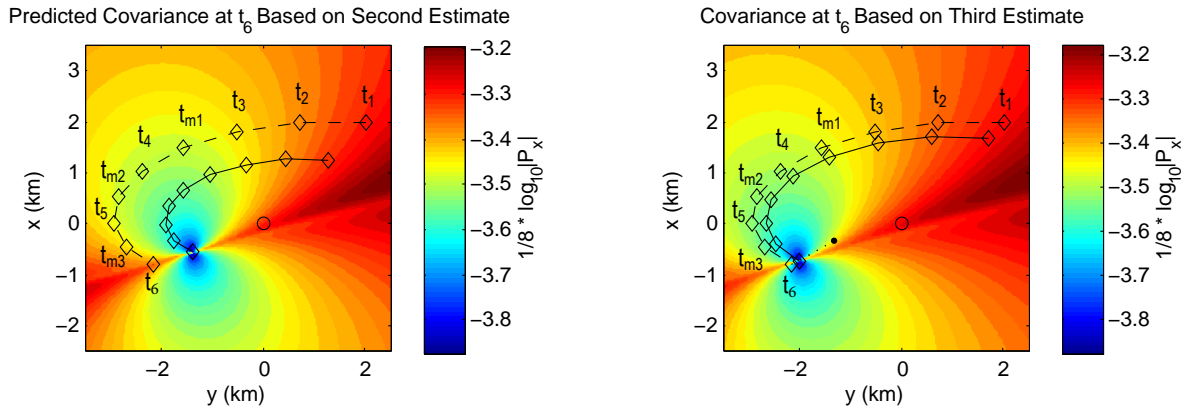


Figure 5.14: Contours of the determinant of (a)  $\mathbf{P}_x(t_6, \hat{x}(t_5), r_{obs}(t_6))$  used to design the second maneuver and (b)  $\mathbf{P}_x(t_6, \hat{x}(t_6), r_{obs}(t_6))$  for after-the-fact reconstruction.

	$\mathbf{x}_0$	$\hat{\mathbf{x}}_0(t_4)$	$\hat{\mathbf{x}}_0(t_5)$	$\hat{\mathbf{x}}_0(t_6)$
<b>r</b>	1.9694	-0.7224	1.2400	1.6607
	2.0285	-0.7473	1.2863	1.7211
<b>v</b>	0.0003	-0.0001	0.0003	0.0004
	-0.0043	0.0016	-0.0027	-0.0036

Table 5.2: Table of true initial states,  $\mathbf{x}_0$  and estimates of initial states  $\hat{\mathbf{x}}_0(t_4)$ ,  $\hat{\mathbf{x}}_0(t_5)$ , and  $\hat{\mathbf{x}}_0(t_6)$ .

## Chapter 6

### CONCLUSIONS

The goal of this work is to develop a method by which to achieve an accurate estimate of an angles-only IROD solution using multiple maneuvers. In the presence of measurement errors, the maneuver design affects the accuracy of the resulting solution estimate. However, prediction of the accuracy obtained by a particular maneuver requires an estimate of the RSO motion itself. For an initial maneuver, no such estimate is available. Instead only a singular direction can be calculated. The possibility of maneuvers that do not alleviate the unobservability of relative motion using angles-only measurements can be calculated, and therefore avoided, using pre-maneuver measurements, or the singular directions can at least be defined to exist in some subspace.

After the first maneuver, an estimate of the RSO motion is available. This estimate can be used to predict the covariance produced from scheduled measurements after candidate maneuvers for the second maneuver. These predictions can therefore be used to design the second maneuver. In a similar manner, the current estimate can be used to design any subsequent maneuvers.

This thesis has demonstrated this approach is effective for obtaining an accurate estimate of RSO motion using angles-only observations, even when the initial estimate is very poor. This approach could be useful for mission planners in performing navigation in proximity operations. In such an application, candidate maneuvers could also be balanced against other priorities such as fuel usage or maneuvering constraints.

## Bibliography

- [1] D. C. Woffinden and D. K. Geller, "Observability Criteria for Angles-Only Navigation," *IEEE Transactions on Aerospace and Electronic Systems*, Vol. 45, No. 3, 2009.
- [2] D. C. Woffinden and D. K. Geller, "Optimal Orbital Rendezvous Maneuvering for Angles-Only Navigation," *Journal of Guidance, Control, and Dynamics*, Vol. 32, No. 4, 2009.
- [3] H. Patel, T. A. Lovell, S. Allgeier, R. Russell, and A. J. Sinclair, "Relative Navigation for Satellites in Close Proximity Using Angles-Only Observations," *AAS/AIAA Space Flight Mechanics Meeting*, 2012.
- [4] B. Newman, T. A. Lovell, E. Pratt, and E. Duncan, "Quadratic Hexa-Dimensional Solution for Relative Orbit Determination," *AAS/AIAA Astrodynamics Specialist Conference*, San Diego, California, August 2014. Paper AIAA 2014-4309
- [5] J. J. Ekelund, "A Means of Passive Range Determination," *Commander Submarine Forces, Atlantic Fleet, Quarterly Information Bulletin*, Summer 1958.
- [6] D. H. Wagner, W. C. Mylander, and T. J. Sanders, eds., *Naval Operations Analysis*, Naval Institute Press, 3 ed., Ch. 11, 1999.
- [7] E. Tse, Y. Bar-Shalom, and L. Meier, "Wide-Sense Adaptive Dual Control for Nonlinear Stochastic Systems," *IEEE Transactions on Automatic Control*, Vol. AC-18, pp. 98-108, April 1973.
- [8] L. M. Hebert, A. J. Sinclair, and T. A. Lovell, "Angles-Only Initial Relative-Orbit Determination via Maneuver," *AAS/AIAA Space Flight Mechanics Meeting*, 2015.
- [9] L. M. Hebert, A. J. Sinclair, and T. A. Lovell, "Singular Maneuvers in Angles-Only Initial Relative-Orbit Determination," *AAS/AIAA Astrodynamics Specialist Conference*, 2015.
- [10] L. M. Hebert, A. J. Sinclair, and T. A. Lovell, "Angles-Only Initial Relative-Orbit Determination via Successive Maneuvers," *AAS/AIAA Space Flight Mechanics Meeting*, 2016.
- [11] H. D. Curtis, "Orbital Mechanics for Engineering Students," Elsevier Ltd., 2 ed., Ch. 7, 2009
- [12] H. Schaub and J. L. Junkins, "Analytical Mechanics of Space Systems," *AIAA, Virginia*, 2003, pp. Sect. 14.3-14.4.

- [13] Carter, T. E., "State Transition Matrices for Terminal Rendezvous Studies: Brief Survey and New Example," *Journal of Guidance, Control, and Dynamics*, Vol. 21, No. 1, pp. 148-155, 1998.
- [14] DeVries, J. P., "Elliptic Elements in Terms of Small Increments of Position and Velocity Components," *AIAA Journal*, Vol. 1, No. 11, pp. 2626-2629, 1963.
- [15] W. H. Clohessy and R. Wiltshire, "Terminal Guidance System for Satellite Rendezvous," *Journal of the Aero/Space Sciences*, Vol. 27, 1960.
- [16] B. D. Tapley, B. E. Schutz, G. H. Born, "Statistical Orbit Determination," Elsevier Academic Press, 2004.
- [17] J. Tschauner and P. Hempel, "Rendezvous zu einem in elliptischer Bahn umlaufenden Ziel," *Astronautica Acta*, Vol. 11, No. 2, pp. 104-109, 1965.
- [18] K. Yamanaka and F. Ankersen, "New State Transition Matrix for Relative Motion on an Arbitrary Elliptical Orbit," *Journal of Guidance, Control, and Dynamics*, Vol. 25, No. 1, pp. 60-66, 2002.
- [19] A. J. Sinclair, R. E. Sherrill, and T. A. Lovell, "Geometric Interpretation of the Tschauner-Hempel Solutions for Satellite Relative Motion," *Advances in Space Research*, 2015. doi: <http://dx.doi.org/10.1016/j.asr.2015.01.032>.